Global Journals LaTeX JournalKaleidoscope™
Artificial Intelligence formulated this projection for compatibility purposes from the original article published at Global Journals. However, this technology is currently in beta. *Therefore, kindly ignore odd layouts, missed formulae, text, tables, or figures.*

Studies on Application of Single Crystal Diamond for Charge Particle Detection: Design, TCAD Simulations, Technology Development, & Dc Characterization

Pourus Mehta[1] and Pourus Mehta[2]

[1] Bhabha Atomic Research Centre

Received: 9 December 2013 Accepted: 5 January 2014 Published: 15 January 2014

Abstract

Single crystal Diamond based Charge Particle detectors have been realized through a pilot stage fabrication run at the Indian Institute of Technology-Bombay (IIT-B). Device simulations in Technology Computer Aided Design (TCAD) were employed to study the physics of charge transport within the detector. Static case simulations revealed values of critical dc performance parameters like total leakage current at applied bias as well as the intrinsic bulk resistance offered by the detector. Dynamic case simulations meant to study the effect of alpha radiation were also conducted. They indicated a certain probability of charge multiplication at low fields within the diamond crystal which needs further experimental investigation to validate. Device simulations also proved helpful in verification and validation of experimental results. Technology for fabrication of diamond detectors was developed through an iterative process spread across several runs to realize a robust device. DC characterization of the fabricated diamond detectors was performed to extract the terminal current at operating voltage (100V), intrinsic bulk resistance of the detector as well as the trend of the I-V curve.

Index terms—

1 Introduction

ingle crystal Diamond (allotrope of elemental Carbon) can be used in very specialized detection applications. The wide Bandgap (5.6 eV at 300 o K) property of diamond imparts it a virtually insulating character at room temperature. This translates into a negligibly low thermal carrier generation rate at room temperature. Thus resulting in very low leakage currents at operating temperatures, in-turn ensuring a low background for the signal and higher quantum efficiency.

For purpose of application of diamond as a detector material, it has to be connected to the electrical circuit. This is normally done by creating metallic contacts on the cubic planar diamond sample by certain specialized methods [1][2][3][4][5]. The fundamental principle behind formation of Ohmic contacts over diamond is to match the work function of the diamond with that of the contacting metal over it.

Author: Electronics Division, Bhabha Atomic Research Centre, MOD Lab, Trombay, Mumbai 400085, India. e-mails: pdmehta@barc.gov.in, pourus_m@yahoo.com

The work function of diamond being ~5eV is within the range of work functions of metals like Titanium (4.33 eV) & Tantalum (4.22 ± 0.06 eV). Hence, either Titanium or Tantalum could be used to make direct contact with diamond films. Additionally, gold films are also deposited over these Ti/Ta films for increased robustness in wire-bonding.

Single crystal Diamond samples were grown by microwave decomposition of methane gas [7]. A piece of single crystal natural diamond was employed as seed for deposition of carbon atoms in a diamond matrix. The seed

crystal was then separated from the epitaxially grown crystal through laser ablation technique. This single crystal diamond sample formed the starting material for realizing Alpha Particle detectors. Proto-type Diamond detectors were realized through a fabrication run at the Electrical Engineering Department, Indian Institute of Technology-Bombay. The technology for fabrication of electrical contacts over diamond crystals was developed through an iterative process. DC characterization of the fabricated devices was performed to establish the current to voltage relationship as well as to know the bulk resistance of the detector.

Additionally, the physics of the alpha particle detection in diamond was studied employing simulation studies in Technology Computer Aided Design (TCAD). The Silvaco Atlas TCAD device simulation suite was employed to perform the simulation studies. The dc characteristics of the detector were simulated to extract the dc bulk resistance of the detector. Dynamic characteristics were simulated by incorporation of a charge cloud equivalent to a deposited energy of 5.5 MeV at a designated lateral distance and time over the two-dimensional cross-section of the diamond detector (Fig. **??**). The output (anode) current pulse w.r.t. time was extracted to study the mechanism of charge carrier transport within the bulk of the detector. Additionally, the energy band diagram in diamond was extracted and confirmed the resistive nature of response in the detector. A p-type, high resistivity, 1 mm thick Diamond substrate forms the starting material for the diamond detector fabrication. To begin with, a virtual 2dimensional cross section of the device had to be defined with the lateral dimension of the diamond structure parallel to the X-axis and the thickness of the crystal to the Y-axis. The 2D cross-section is then further sub-divided into rectangular unit cells by definition of a mesh/grid structure which covers the entire physical simulation domain. Meshes can be of three types viz. rectangular, cylindrical and triangular. The first two types are defined in two dimensions whereas the cylindrical mesh can only be defined in 3D structure. A rectangular mesh is essentially a matrix of horizontal and vertical lines spaced at pre-defined distances across the entire physical space. Specification of mesh involves a tradeoff between the requirements of accuracy, numerical efficiency & time economy.

2 S

3 Global

A good degree of accuracy demands definition of a finer mesh to resolve minute features of the structure. Time economy entails the requirement of a coarse mesh to minimize total number of grid points and reduce simulation time. Mesh definition is something that requires sufficient skill and experience in understanding the finer nuances of using the simulation tool. Some of the guidelines that can be helpful in creating a good grid are as follows.

? A mesh should be such that it has the minimum number of grid points to provide the required accuracy at the same time does not have too many excess points which impose a cost on time economy. ? During mesh generation there is fair probability of generating obtuse triangles which can impair accuracy, convergence, and robustness. Hence, the mesh should be defined in such a way so as to minimize the number of obtuse triangles (preferably $< 1\%$ of number of triangles).

? While defining a mesh, care should be taken to minimize long thin triangles which create problems of convergence.

After definition of a mesh there are sufficient provisions to improve the mesh to achieve accuracy and time economy. Mesh improvement algorithms have to be employed to improve inconsistencies in a coarse mesh. There are two techniques available for mesh refinement viz. node smoothing and triangle smoothing. With node smoothing, several iterative passes are carried out during, which each node is moved to a position and improves the angles of the triangles surrounding it. Node smoothing should only be used for grids that are already irregular. If node smoothing is used for nearly rectangular grids, it may significantly degrade the quality of the mesh.

In triangle smoothing (which is also referred to as diagonal flipping), each adjoining pair of triangles is examined. If appropriate, the diagonal of the gas. The first proto-type of diamond detectors (Fig. **??**) quadrilateral is flipped to stabilize the discretization. The diagonal is never flipped when two elements are composed of different materials. Triangle smoothing is desirable in almost all cases, and should be performed on both the initial grid and in subsequent regrid regimes. There is fair probability of generation of errors associated with a mesh generation which can be eliminated by systematically repeating the calculation using a sequence of progressively finer meshes. The typical approach is to adequately resolve structural features, including doping, with an initial or base mesh, and then add nodes as required to resolve significant features of the solution. Definition of meshes in ATLAS can be through various routes. Firstly, a pre-generated mesh used in a process simulation program can be directly inherited into the device simulator. Secondly, meshes can be defined analytically by specification of X-Y co-ordinates of every point in the 2 dimensional cross-section which gives greater grid control to the designer.

Mesh can also be generated through a special purpose device generation utility called DEVEDIT available in the tool which is a GUI based program that can employed to interactively define the meshes together with definitions of the various regions of the device. The mesh for the 2D structure of the diamond detector was generated with a maximum of 20,000 grid points (grid point limit). The grid density worked out to be 0.01 points/Area, which was the maximum possible density for this structure. The 2-dimensional crosssection of the diamond detector is illustrated in Figure **??**. Once the mesh has been generated and tuned for good accuracy, the next job is to define various regions like diamond, metals, etc. at specific locations of the 2-dimensional

cross-section. As seen from figure **??**, the diamond substrate is defined by a rectangle from x = 0 µm -2000µm and y = 0 µm -1000 µm. Metallic contacts were defined over both the top (y = 0) and bottom faces (y = 1000).

depth. The one dimensional doping profile along the depth (Y-direction) of the device is illustrated in figure 3. Subsequently, electrical contacts were formed by titanium deposition at the top and bottom surfaces of the diamond crystal to form Anode and Cathode electrodes respectively.

Boron exists in natural Diamond as an acceptor impurity (E av =0.37eV) on a substitutional site. To incorporate this, boron dopant needs to be defined within the semiconductor bulk. The p-type impurity was incorporated within the bulk of the diamond lattice with a uniform doping concentration of 5.43x10 7 cm -3 along the The processes responsible for generationrecombination can be broadly categorized into phonon transitions, photon transitions, Auger transitions, surface recombination, impact ionization & tunneling. Phonon transitions occur in the presence of a trap (or defect) within the forbidden gap of the semiconductor. This is essentially a two step process, the theory of which was first derived by Shockley and Read and then by Hall. The Shockley-Read-Hall recombination is modeled as follows.

()**2**

Where ETRAP is the difference between the trap energy level and the intrinsic Fermi level, TL is the lattice temperature in degrees Kelvin and TAUN0 and TAUP0 are the Electron and Hole lifetimes. T L is the lattice temperature, p & n the hole and electron densities resp.

The Shockley Read Hall and Auger recombination models pertaining to generation/recombination processes were incorporated.

Carriers (Electrons/holes) get accelerated by application of electric fields. There are inherent Processes of generation-recombination restore the semiconductor material to equilibrium after the perturbation force ceases to exist. A homogeneously doped semiconductor with carrier concentrations n and An optimized value of minority carrier lifetime of 5 ms was achieved for which the total current at 100V applied bias was 80nA as was the case in experimental I-V characteristics. Similarly, the values of Electron and Hole mobility were set to 500 cm 2 /V.s and 300 cm 2 /V.s respectively by iterative derivation and matching I-V curves from simulation with experiment. mechanisms in nature to restore balance in materials. These processes scatter the accelerated charges and dissipate the energy and thus leading to a reduction of linear momentum. Scattering mechanisms can be broadly classified as lattice scattering (phonons assisted) and impurity scattering. The cumulative effect of all these restoring mechanisms on the macroscopic scale leads to a reduction in overall mobility of carriers. Mobility models are defined for low-field behavior & high field behavior. The low electric field behavior pertains to carriers being near equilibrium. The high electric field behavior shows that the carrier mobility decreases with increase in electric field. The mean drift velocity no longer increases linearly with increasing electric field, but saturates to a value denoted by V SAT .

The field dependent mobility is related to the low field mobilities (µ n0 and µ p0) according to the following equations.

() (4)**3**

Where "E" is the parallel electric field and µ n0 and µ p0 are the low-field electron and hole mobilities respectively. Modeling mobility in bulk material involves: (i) characterizing µ n0 and µ p0 as a function of doping and lattice temperature, (ii) characterizing V SAT (Saturation Velocity) as a function of lattice temperature, and (iii) describing the transition between the low-field mobility and saturated velocity regions. The parallel Field Dependent Mobility model (Equations) was incorporated which constitutes the modeling of velocity saturation effects in high field devices.

Numerical solutions to the Poisson and continuity equations (Eq.) now need to be deduced. There are various numerical methods like Newton (Block & Autonr), Gummel, etc. which can be employed. The Newton-Richardson Method is a variant of the Newton method that calculates a new version of the coefficient matrix only when slowing convergence demonstrates that this is necessary. An automated Newton-Richardson solution can be deduced by invoking the AUTONR parameter available in ATLAS, which improves performance significantly. Convergence is the primary prerequisite for achieving accuracy in numerical solution to the problem. Various strategies like bias update size reduction can be employed to achieve convergence quickly. Newton's method is the default for drift-diffusion calculations in ATLAS as it is fairly accurate in dc, transient, curve-trace analysis & frequency-domain small-signal analysis.

Subsequently, certain boundary conditions viz. Ohmic, Schottky, insulated and Neumann (reflective) need to be specified for definition of the electrical nature of biasing electrodes. Voltage and current boundary conditions are normally specified at most kinds of electrodes. In this case, both electrodes (anode & cathode) were attributed to a voltage boundary condition to simulate Ohmic nature of these electrodes as in actual measurement. Poisson and continuity equations were solved at every grid point with appropriate initial guesses using Newton-Richardson method. The dc voltage on the anode was ramped from 0 V to +100 V keeping the cathode at ground potential. The dc characteristics were extracted for the first quadrant of the I-V characteristics. Subsequently, a reverse bias of -100V was applied to the anode to simulate the nature of the I-V in reverse direction.

In the dynamic simulations case, special charge generation models had to be incorporated to emulate charge carrier generation by sub-atomic charge particles in Diamond. An alpha particle incidence simulation was performed employing the Single-eventupset (SEU) command set for emulating a charge density within the active volume of the diamond crystal. SEU command line features options in controlling various parameters of the

simulation. An alpha particle track of specific radius (R) and energy can be defined to pass through the cross-section of the device at a Global Journal of Researches in Engineering ( ) designated X location and for a specific track length in Y direction. Electron/hole pairs generated at any point are a function of the radial distance "r" from the center of the track to the point, the distance "l" along the track and the time of incidence "t". The implementation into ATLAS allows definition of the generation rate as the number of electron-hole pairs per unit volume along the track according to the following equation.

4 (, ,) * 1( ) * . * 2 () * ( ) * ( ) G r l t DENSITY L l S B DENSITY L l R R T t = +

DENSITY and B.DENSITY are defined as the number of generated electron/hole pairs per cm 3 . Scaling factor denoted by "S" is given by the following equation.2 1 S q RADIUS ? =**(9)**

The factors L 1 and L 2 are defined according to equation.4 * 1 1 2 3 ( ) * A l L l A A l A e =+ + (**10**) 4 2 1 2 3 ( ) (*) B L l B B l B l = +**(11)**

Parameters A 1 , A 2 , A 3 , A 4 , B 1 , B 2 , B 3 , and B 4 are user-definable and can be tuned for optimization purposes.

An alpha particle track of 1µm radius was defined at a distance of 500µm from the leftmost edge of the device in the X-direction (500,0.0,0.0; 500,21.0,0.0). The e-h pair number density (N o = Number of e-h pairs / Volume) was fixed to be 6.419 x 10 15 cm -3 corresponding to a volume of 6.59 x 10 -11 cm 3 for an alpha particle track length of 21 µm in Prior to running the iterative solver for alpha particle incidence, the dc solution for an applied bias of 100V had to be obtained using the static simulation regime already explained previously. Once the detector was biased at 100V, a transient simulation could be performed for the dynamic case. A time variant simulation was performed for a total simulation time of 100µs. Time steps were tuned in a way to provide finer (0.2ps) time variation at time of alpha incidence for better accuracy in resolution of the dynamic behavior of the device. Solutions were obtained using the Newton method with additional specification of minimum (10fs) & maximum time step (0.2ps) for the entire simulation.

At various stages output files were generated to obtain parameters like electric field, electron/hole velocity, electric field lines/vectors, electron and hole current densities & conduction/valence band edges.

Diamond [Range of 5.5 MeV Alpha in Diamond = 21 µm (SRIM Database)]. The simulation was performed for a total time of 100 µs with an alpha particle incidence time being 10 pico-seconds and a pulse width of 1.28 picoseconds corresponding to the 21µm trajectory in diamond. All material specific parameters like lifetime, mobility etc. remained the same as in the static simulation case. Models pertaining to mobility and generation/ recombination were the same as in the static simulation case.

5 b) Results & Discussions

The 2D cross-section of the diamond detector [Fig. **??**] has been subjected to application of appropriate voltages and suitable boundary conditions (discussed in previous section) to ensure that the solution to the Poisson & continuity equations converged. Biases were applied such that the back-cathode was at a zero potential whereas the anode potential was varied from -100 V to 100 V. Application of such biasing scheme developed a linear potential distribution along the depth (Fig. **??**: Y-direction) of the detector. The reciprocal of slope of simulated I-V (Fig. **??**) curve gave the bulk resistance which worked out to be 1.3 G?. The trend of the I-V characteristic was linear indicating an Ohmic nature of the dc response of the detector. The twodimensional potential contour plot (Fig. **??**) showed a linear gradation of the potential along the depth of the detector whereas across the lateral dimension (Fig. **??**: X-direction) it is equipotential in nature. The electric field vector plot (Fig. **??**) shows a vector direction pointing from anode to back-cathode indicating an electron movement from cathode to anode. The second rung of simulations was performed to parameterize the dynamic response of the diamond detector to alpha radiation. An alpha particle pulse simulation was performed by defining an ionization charge track of 1µm radius at a lateral distance (X-direction) of 500µm from the leftmost edge of the cross-section. The number of generated electron-hole pairs analytically worked out to be 4.23 x 10 5 corresponding to an alpha energy of 5.5 MeV (e-h pair generation energy in diamond = 13eV). The photogenerated electrons got swept across the constant Electric Field (1000 V/cm) towards the anode (+ve Electrode) for an applied potential difference of +100 V w.r.t back-cathode. Corresponding to the field strength of 1000 V/cm & Electron Drift Velocity of 5×10 5 cm/s, the Electron Mobility worked out to be 500 cm 2 /V.s at 300 o K. This implied a total response time (Drift Time) of 200ns for a drift distance of 1000 µm (thickness of substrate).

Dynamic simulations gave the dynamic current output of the detector at the anode as shown in figure **??** (a). The incident alpha particles underwent a columbic interaction with diamond resulting in ionization of the target material along the track. The anode current characteristics (Fig. **??**a) showed two distinct features, the first one began at 8 ps and peaked at 12 ps to a value of 0.65 mA above the dc baseline of 80 nA at 100 V applied bias. The first feature (fast-component) is due to the collection of alpha generated electrons at the top-surface which is exposed to the alpha radiation. The area under the curve of the first feature of the current pulse resulted in a deposited a total charge of 64.8 fC within the bulk of the diamond lattice (Fig. **??**-a). Figure **??** displayed the value of deposited charge to be 67.5 femto-Coulomb. The analytically derived alpha deposited charge worked out to be 65 femto-Coulomb which was in good agreement with that derived from simulation (Fig. **??**). The second

feature of the alpha characteristics (slow-component) begins to develop at 100 nanosecond and attains a value of 30µA at a time of 1 µs. The second feature of the anode current pulse characteristics can be attributed to the drift and ultimate collection of holes (primary ionization charges) at the back-cathode.

6 Global Journal of Researches in Engineering

The total area under the curve for the anode pulse characteristics (including slow and fast components) worked out to be 41 pico-Coulombs. This value of charge was very much higher than deposited primary charge of 67 femto-coulombs indicating the probability of existence of secondary ionization within the bulk of the diamond lattice. The simulated current pulse showed a good resemblance to the experimentally derived pulse displayed in reference 10. The probability of secondary ionization can be higher for holes due to their higher effective mass as compared to electrons at the same energy. Figure **??**(b) shows that the slow component at 1 µs is entirely contributed due to the collection of generated holes at the back electrode. The calculated charge gain factor worked out to be 611 per deposited primary hole. Further exhaustive experimental studies are required to prove the proposed concept of charge multiplication within diamond lattice at low field.

The total collection time for the entire generated charge (primary and secondary) was 2.5 micro-seconds at a detector bias of 100V. The electron current density contours and vector plots (Figs. 9 & 10) showed a peak density at the point of alpha particle incidence (500µm) along the lateral dimension of the detector. This confirmed the existence of alpha particle induced electron-hole pair generation within the bulk of the detector. The energy band diagram (Fig. **??**1) in the bulk of the diamond is linear and maintains a band-gap of 5.5eV which confirms a resistive response for the detector. Single-crystal Diamond samples were grown using Plasma assisted CVD technique, over a commercial, <100> oriented polished single-crystal diamond substrate [7]. Prior to undergoing any growth process, these single crystal diamond substrates were subjected to hydrogen plasma treatment for surface topology linearization. Subsequently, the growth of <100> oriented carbon mono-layers in a diamond matrix was initiated at a temperature of 1000 o C employing 8% methane as precursor gas in a hydrogen ambient, at 140 Torr of total gas pressure. The growth rates varied from 10-15 µm/h depending on a microwave power variation from 1 and 2kW.

7 Global Journal of Researches in Engineering

This sample of single crystal diamond formed the starting material for detector development. A 12 nm thick Titanium film was deposited over the Diamond crystal by plasma sputtering technique (Nordiko Sputter System). This was followed by deposition of a 170 nm thick gold film over the existing Titanium film for reasons discussed earlier. Subsequently, the crystal metallized on both opposite faces was subjected to annealing treatment at 775°C for 60 minutes in nitrogen atmosphere to prevent the high temperature allotropic transformation of diamond to graphite. Titanium forms Titanium Carbide after reacting with diamond. This lead to a minimization of the work function difference between diamond and Ti and in turn imparting Ohmic character to the contact. Other methods of Ohmic contact formation were not feasible as they required the boron implantation facility which was unavailable on site.

V.

8 Dc Characterization a) Objectives & Measurement Methodology

I-V characterization of the diamond detector was performed to extract the dc leakage current across the device at room temperature. The leakage current forms the dc baseline of the alpha particle generated pulse in the detector. The dimensions of the diamond crystal being small, handling became quite an issue. To prepare the detector for characterization required the manufacture of a special enclosure/Test-zig (Fig. 12) to house the device. The enclosure was essentially a cylindrical cavity with a lid to which a co-axial BNC connector was attached. The outer casing of the BNC connector was electrically connected to the metallic enclosure. The central electrode of the BNC was attached to a gold coated copper probe at its extremity. The diamond detector was placed with one of its goldcoated electrodes making contact with the bottom face of the cavity and placing the lid over the cavity biased the top gold-coated electrode. The required bias was applied to the central electrode of the BNC connector w.r.t the external casing which was being held at ground potential. A Keithley 2400 source-measure unit (SMU) was employed to bias the detector. A computer based GPIB program was coded to run the automated dc I-V characteristics.

9 Conclusions

First prototypes of single crystal Diamond based Alpha detectors have been successfully fabricated at IIT-Bombay. Technology for fabrication of diamond detectors has been developed at IIT-Bombay. Physics based simulations in TCAD proved helpful in understanding the charge transport mechanism within the bulk of the diamond detector. Device simulations yielded a bulk resistance of 1.33 G? and also confirmed Ohmic response of the detector. Dynamic simulations incorporating alpha particle incidence played a crucial role in studying the

charge generation mechanism within the diamond crystal. Dc characterization of diamond detectors yielded a terminal dc current value of 82 nA at 100V implying a bulk resistance of 1.30 G?.

Analytical values of dc performance parameters derived from TCAD simulations were found to be having a deviation <5% from those achieved by characterization. Exhaustive dynamic characterization studies on Diamond detectors employing radiation sources (241 Am) are to be taken up shortly.

10 VII. Acknowledgments

The author expresses a deep sense of gratitude for Late Dr. S. K. Kataria for his guidance and leadership. In addition, he would also like to thank Prof. D.S. Misra, Prof. Raghav Verma & Dr. Dipti Ranjan Mohapatra from Physics Department, Indian Institute of Technology -Bombay for their support in this project. The author would like to especially thank Mr. V.D. Srivastava, Mr. V.B. Chandratre from BARC for their kind support. In addition, he would also like to thank Prof. Ramgopal Rao, Prof. Dinesh Sharma & Prof. Apte from the Electrical Engineering Department, Indian Institute of Technology -Bombay for their guidance and support.

Figure 1:

1 2

[1]© 2014 Global Journals Inc. (US)

[2]Year 2014 © 2014 Global Journals Inc. (US) Studies on Application of Single Crystal Diamond for Charge Particle Detection: Design, TCAD Simulations, Technology Development, & Dc Characterization

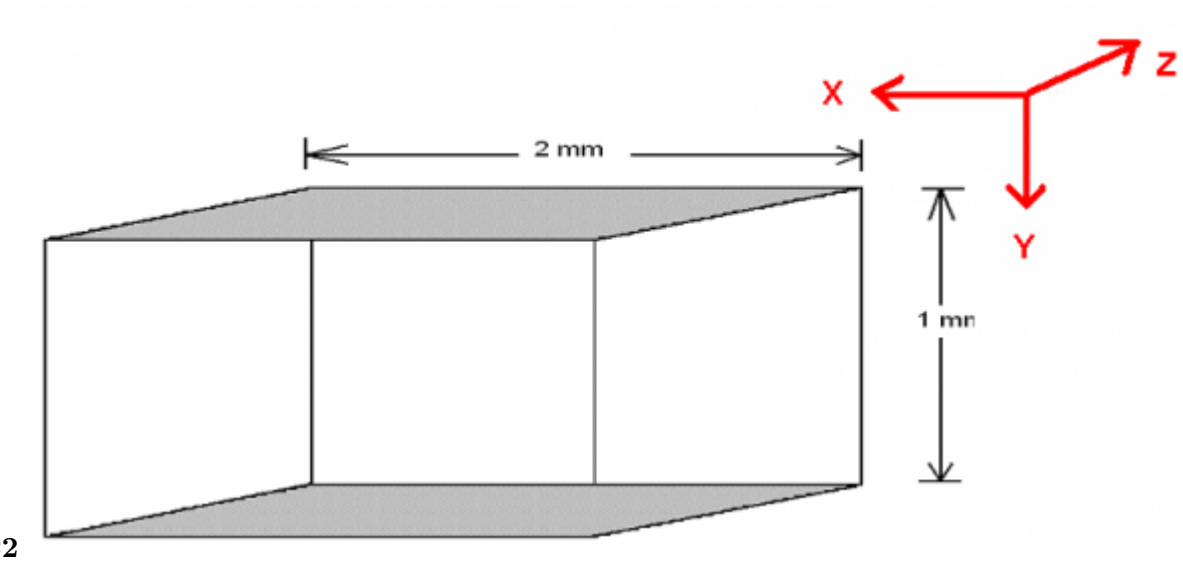

22

Figure 2: Fig. 2 : 2 -

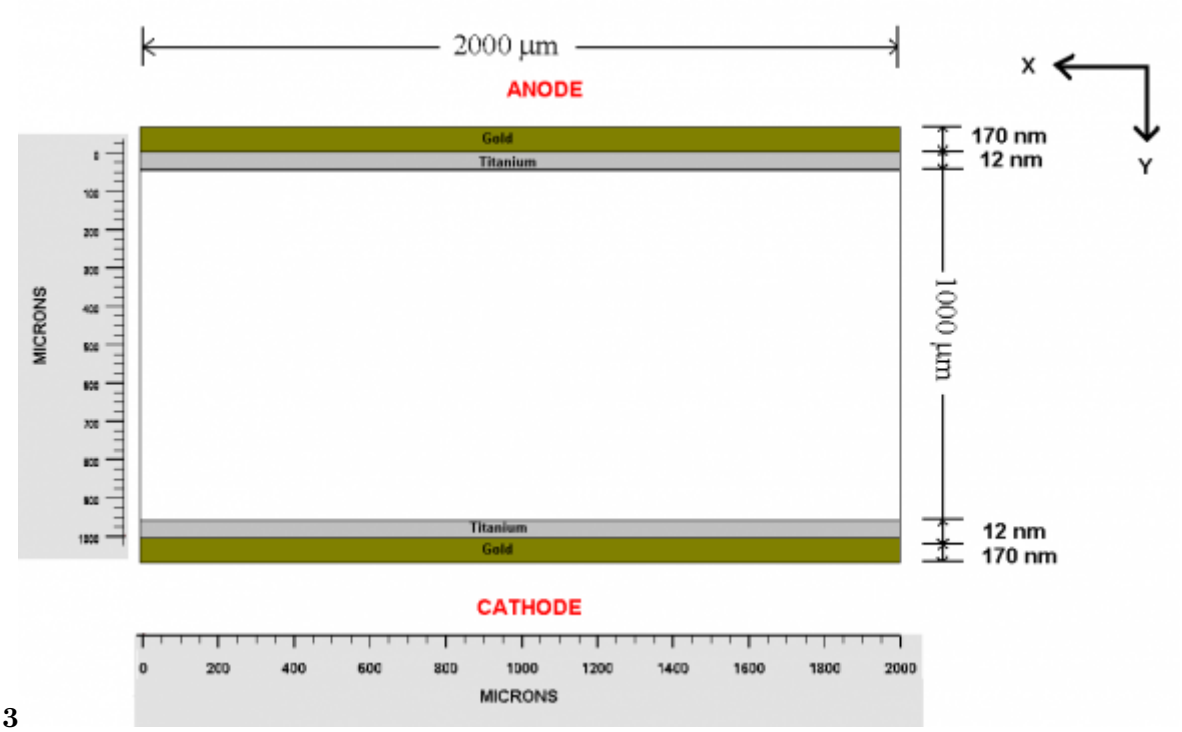

3

Figure 3: Fig. 3 :

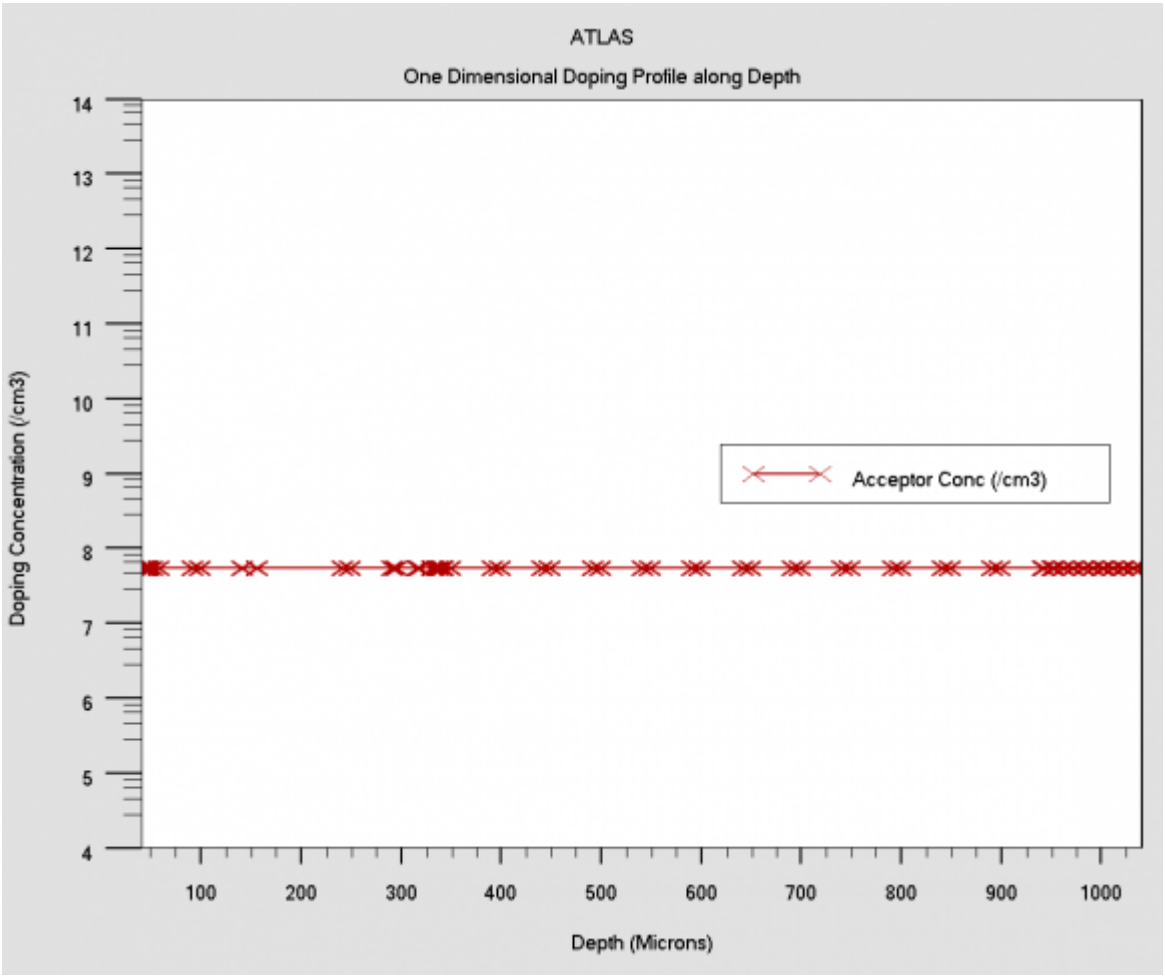

Figure 4:

$$R_{SRH} = \frac{pn - n_{ie}^2}{\mathrm{TAUP0}\left[n + n_{ie} exp\left(\frac{\mathrm{ETRAP}}{kT_L}\right)\right] + \mathrm{TAUN0}\left[p + n_{ie} exp\left(\frac{-\mathrm{ETRAP}}{kT_L}\right)\right]}$$

46

Figure 5: Fig. 4 :Fig. 6 :

$$\mu_n(E) = \mu_{n0}\left[\frac{1}{1 + \left(\frac{\mu_{n0}\, E}{\mathrm{VSATN}}\right)^{\mathrm{BETAN}}}\right]^{\frac{1}{\mathrm{BETAN}}}$$

$$\mu_p(E) = \mu_{p0}\left[\frac{1}{1 + \left(\frac{\mu_{p0}\, E}{\mathrm{VSATP}}\right)^{\mathrm{BETAP}}}\right]^{\frac{1}{\mathrm{BETAP}}}$$

78

Figure 6: ()Fig. 7 (Fig. 8 :

$$\frac{\partial n}{\partial t} = \frac{1}{q} div \vec{J}_n + G_n - R_n$$

$$\frac{\partial p}{\partial t} = -\frac{1}{q} div \vec{J}_p + G_p - R_p$$

911

Figure 7: ()Fig. 9 :Fig. 11 :

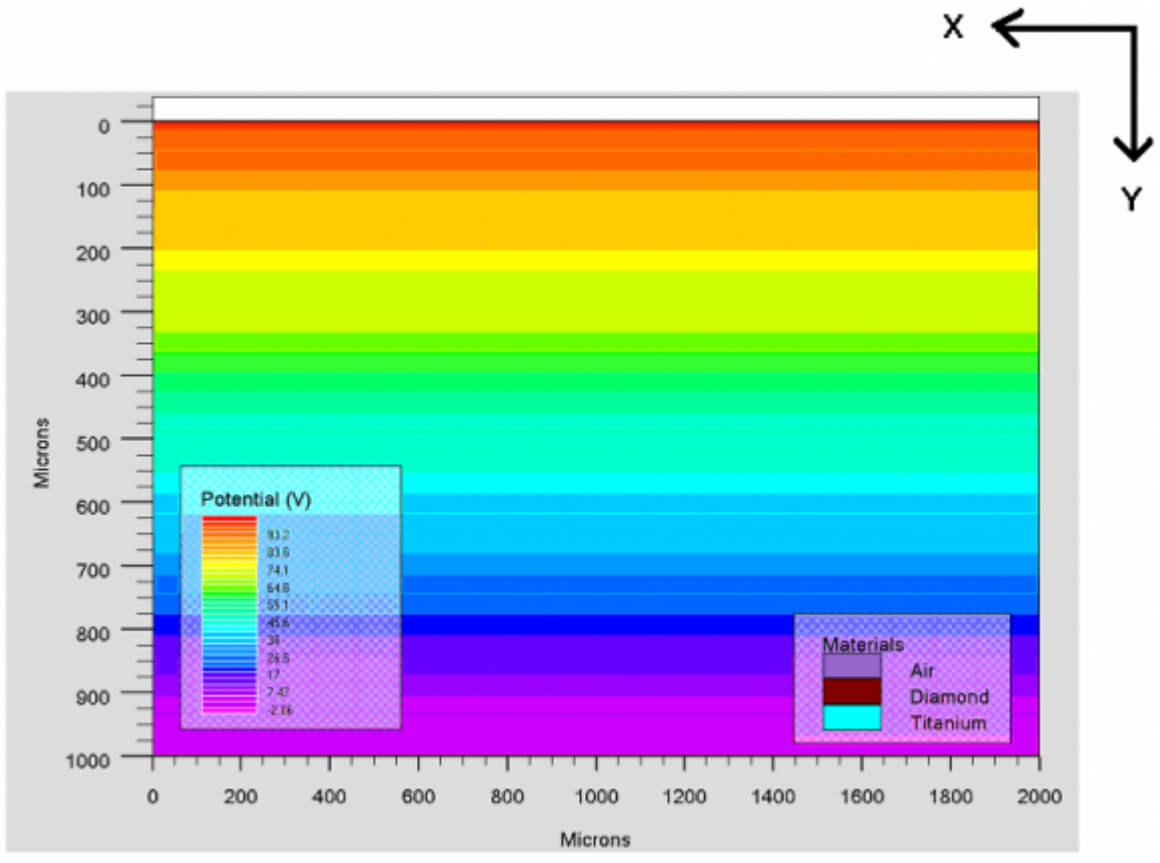

12

Figure 8: Fig. 12 :

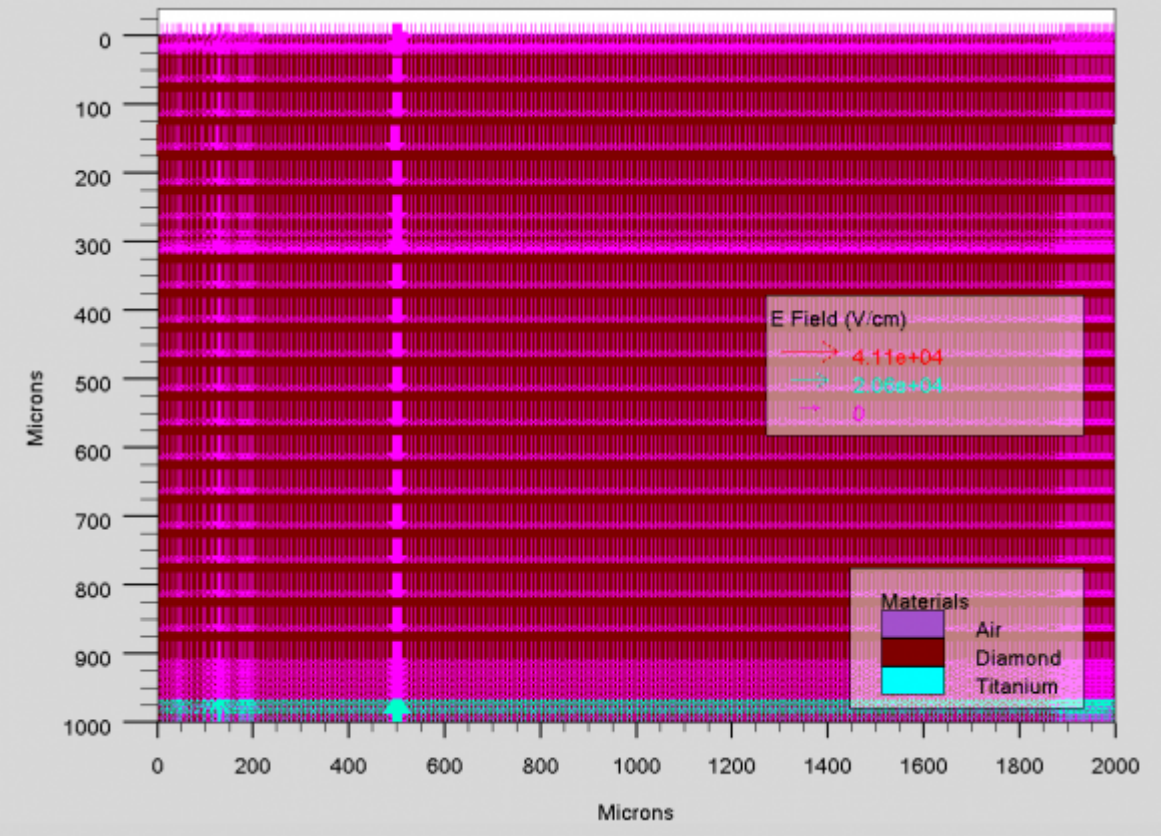
E Field (V/cm)
4.11e+04
2.06e+04
0
Materials
Air
Diamond
Titanium
Microns
Microns
0
100
200
300
400
500
600
700
800
900
1000
0
200
400
600
800
1000
1200
1400
1600
1800
2000

Figure 9:

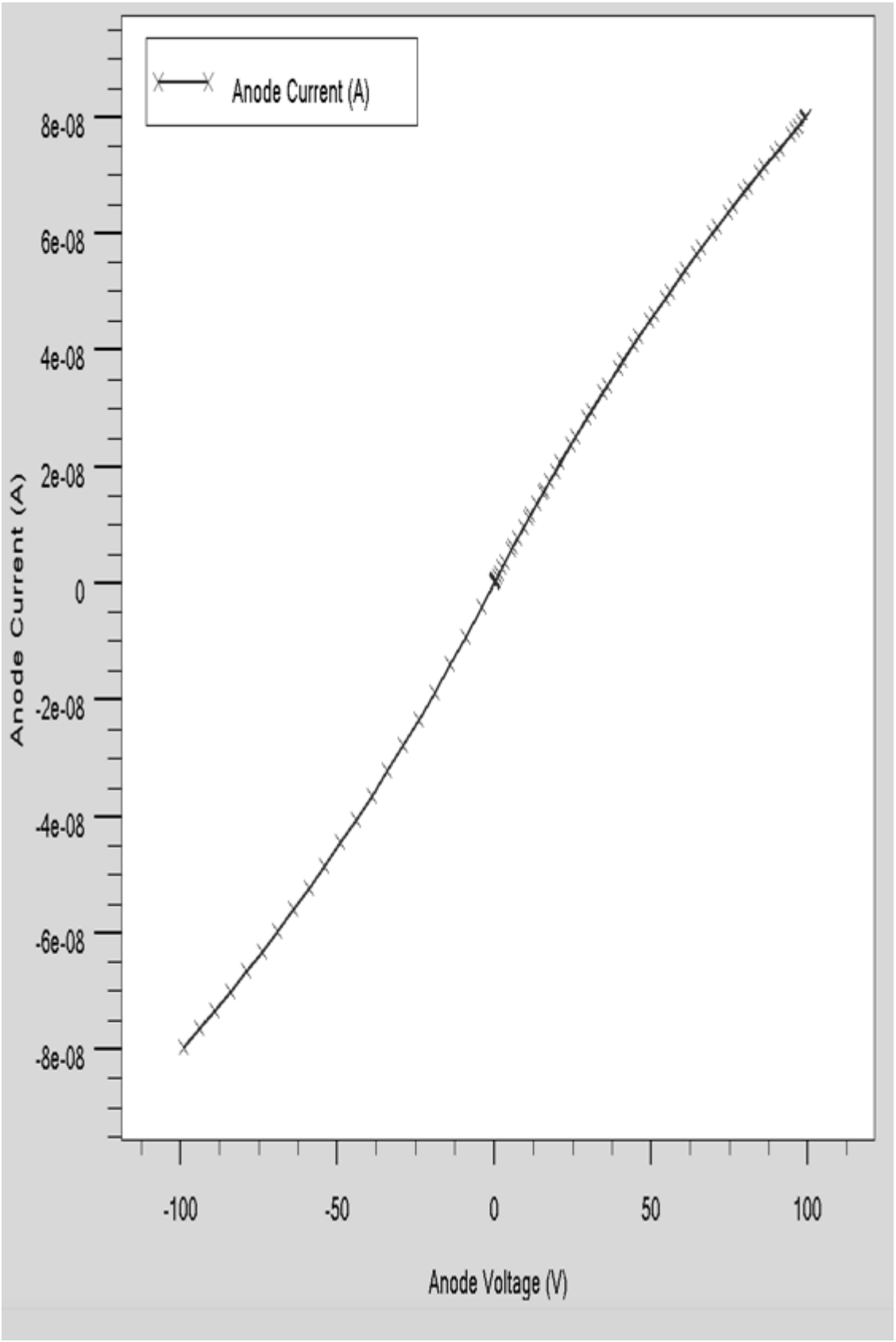
Anode Current (A)
8e-08
6e-08
4e-08
2e-08
0
-2e-08
-4e-08
-6e-08
-8e-08
Anode Current (A)
-100
-50
0
50
100
Anode Voltage (V)

Figure 10:

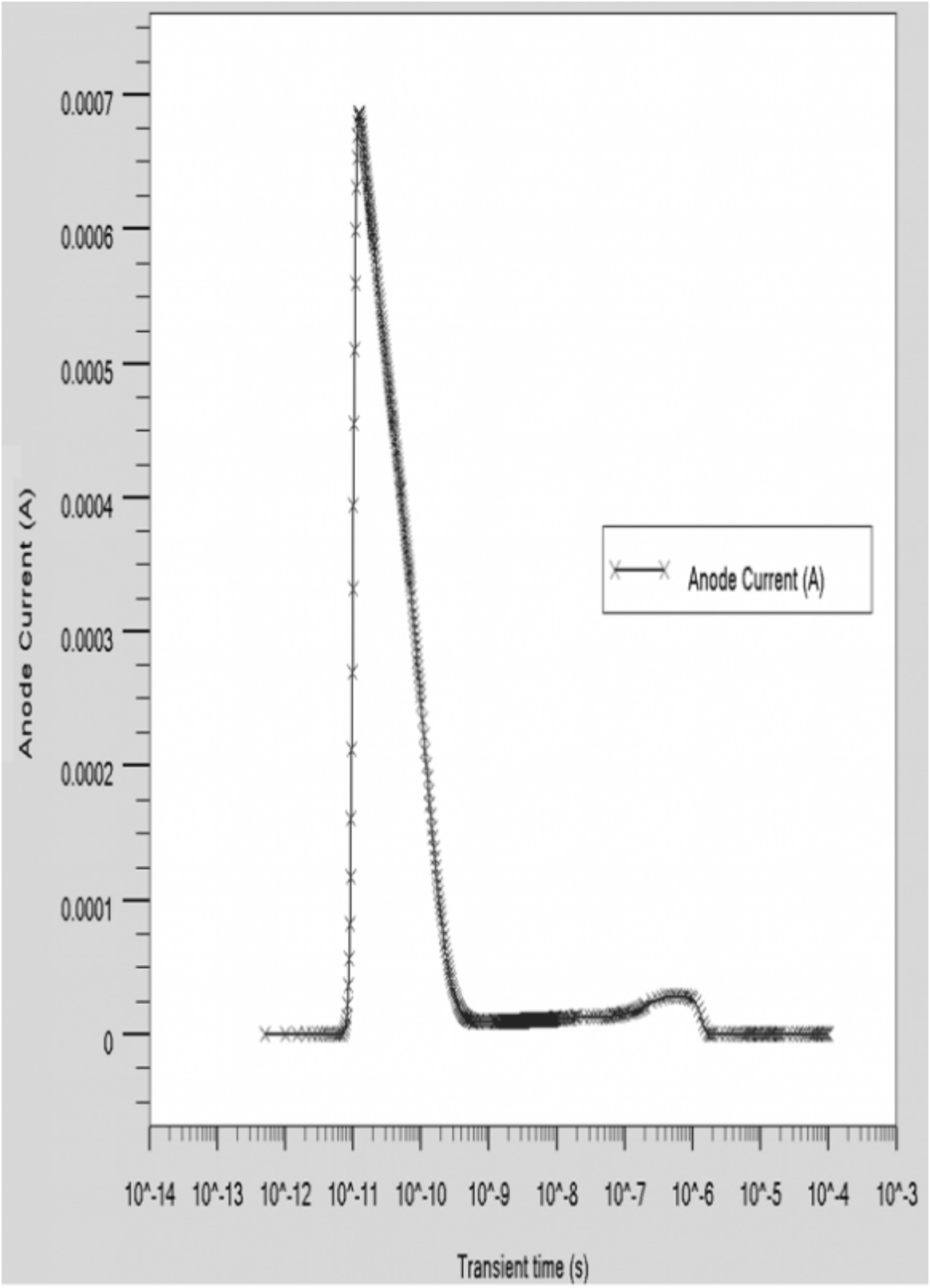
0.0007
0.0006
0.0005
0.0004
0.0003
0.0002
0.0001
0
Anode Current (A)
Anode Current (A)
10^-14 10^-13 10^-12 10^-11 10^-10 10^-9 10^-8 10^-7 10^-6 10^-5 10^-4 10^-3
Transient time (s)

Figure 11:

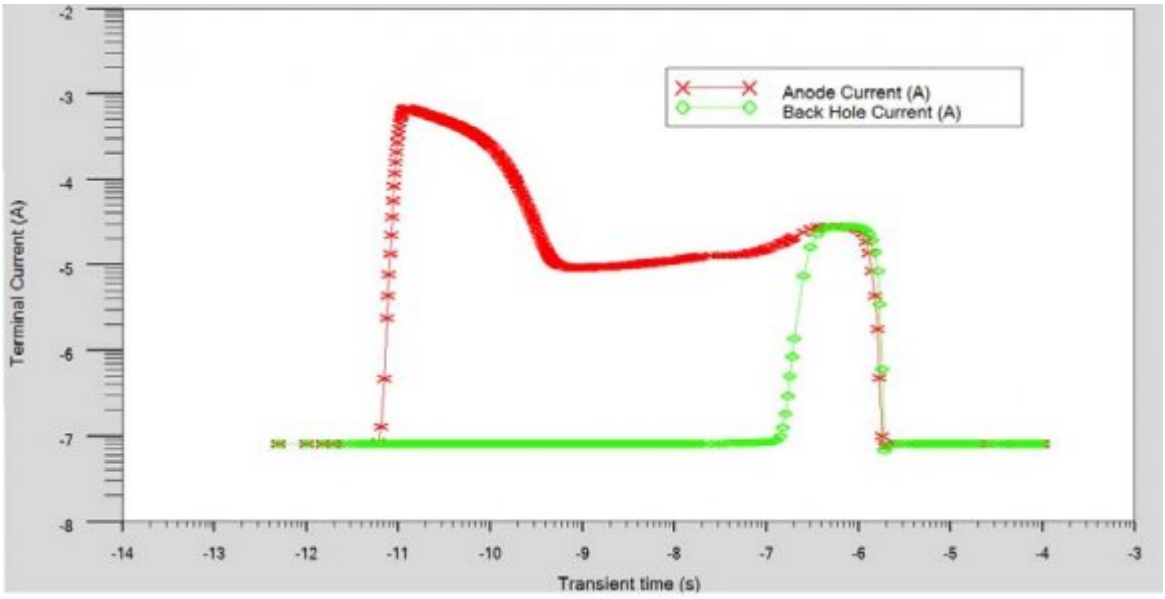
Anode Current (A)
Back Hole Current (A)
Terminal Current (A)
Transient time (s)
-2
-3
-4
-5
-6
-7
-8
-14
-13
-12
-11
-10
-9
-8
-7
-6
-5
-4
-3

Figure 12:

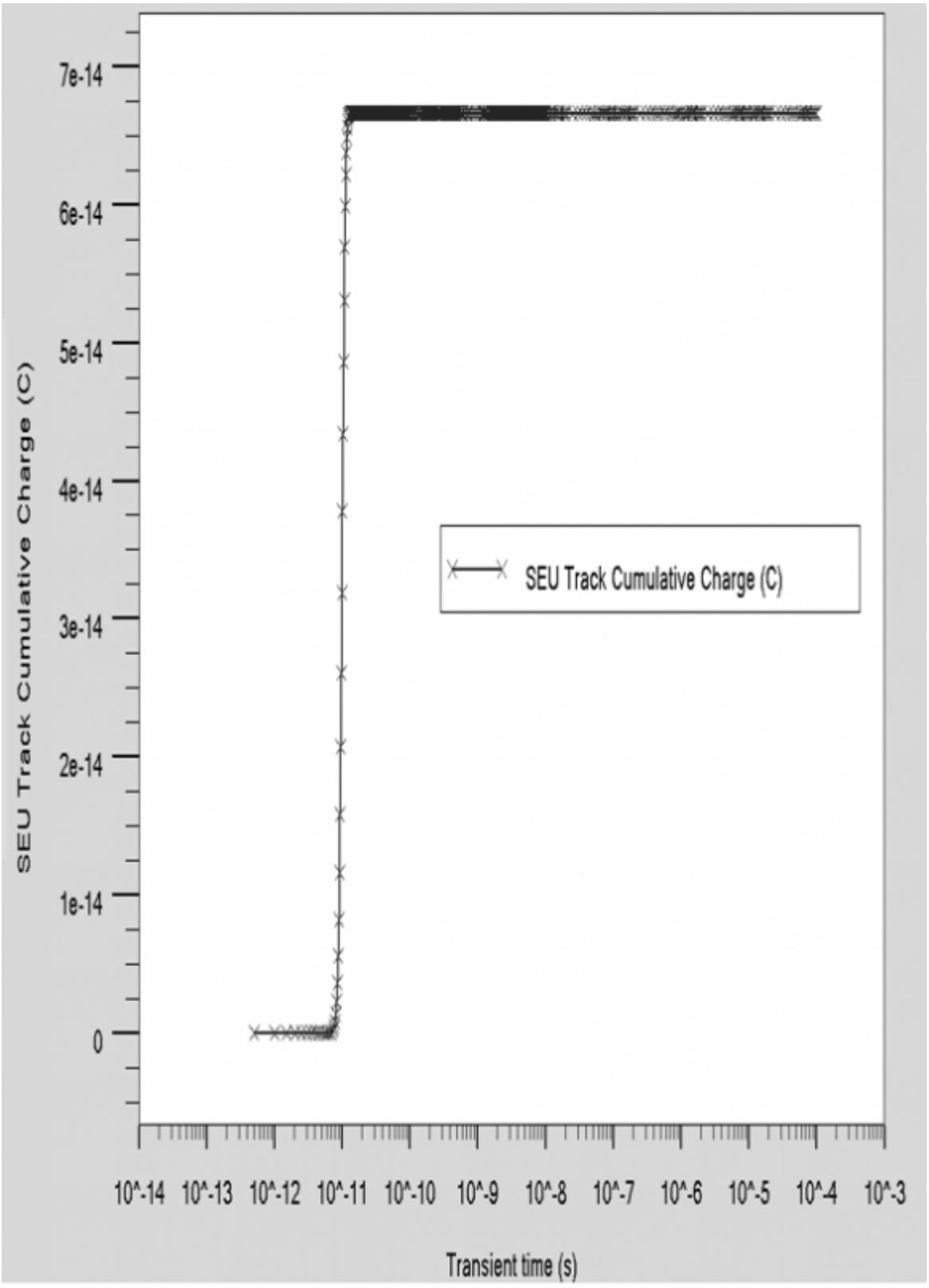
7e-14
6e-14
5e-14
4e-14
3e-14
2e-14
1e-14
0
SEU Track Cumulative Charge (C)
SEU Track Cumulative Charge (C)
10^-14 10^-13 10^-12 10^-11 10^-10 10^-9 10^-8 10^-7 10^-6 10^-5 10^-4 10^-3
Transient time (s)

Figure 13:

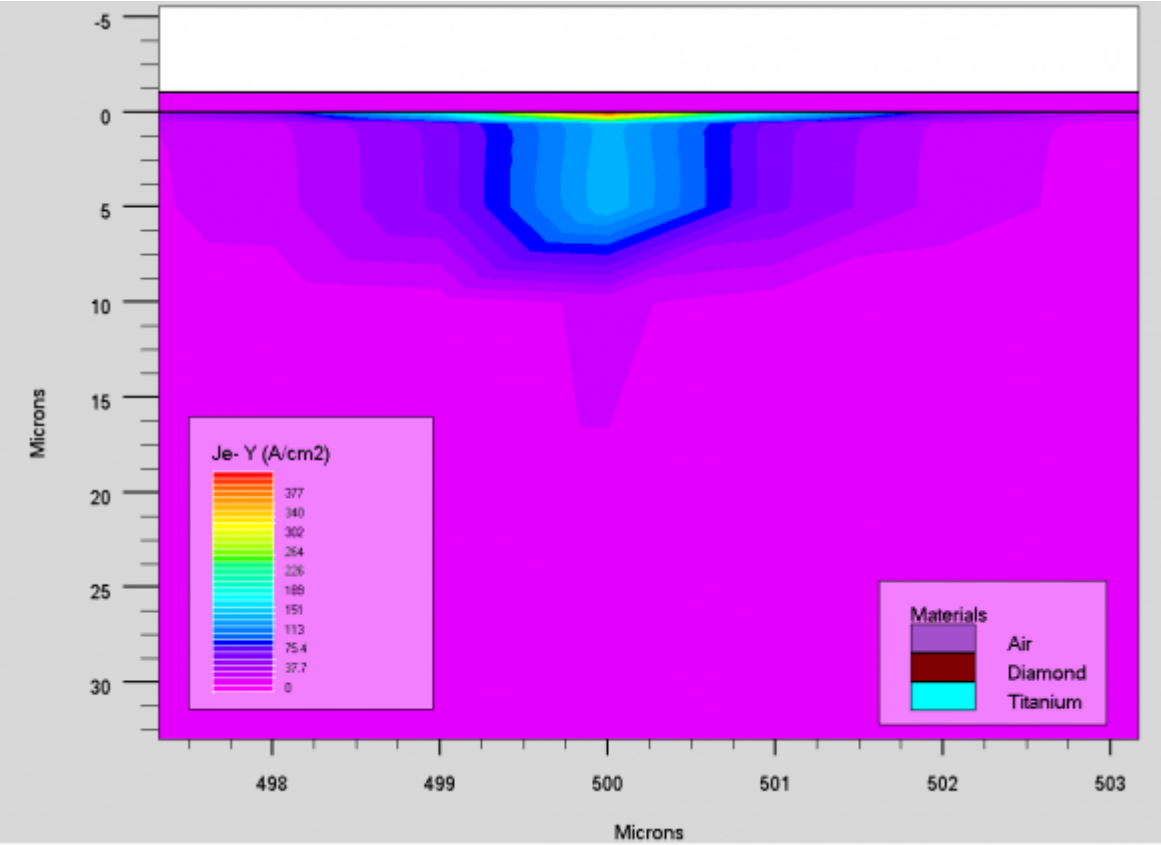
-5
0
5
10
15
20
25
30
Microns
Je- Y (A/cm2)
377
340
302
264
226
189
151
113
75.4
37.7
0
Materials
Air
Diamond
Titanium
498
499
500
501
502
503
Microns

Figure 14:

[ATLAS user manual] , *ATLAS user manual*

[Rinat et al.] 'Conductivity in boron-doped diamond'. F Rinat , Takashi Mamin , Inushima . *Physical Review B* 63 p. .

[Tachibana et al.] 'Correlation of Electrical Properties of Metal Contacts on Diamond Films with Chemical Nature of Metal-Diamond Interface, Gold Contacts: A Non-Carbide Forming Metal'. T Tachibana , B E Williams , J T Glass . *Physical Review B* 45 (20) p. 968.

[Dipti Ranjan Mohapatra ()] 'Development of Crystallographic Texture and In-Grain Misorientation in CVD-Produced Single and Polycrystalline Diamond'. Dipti Ranjan Mohapatra . *Journal of Chemical Vapour Deposition* 2011. 17 p. .

[Walker et al. ()] 'Formation of buried p-type conducting layers in diamond'. R Walker , S Prawer , D N Jamieson , K W Nugent . *Appl. Phys. Lett* 15 September 1997, 1492. 71 (11) .

[Isberg and Gabrysch ()] 'High-field Electrical Transport in Single Crystal CVD Diamond Diodes'. J Isberg , M Gabrysch . *Advances in Science and Technology* 2006. 48 p. .

[Lake Shore 7500/9500 Series Hall System User's Manual] *Lake Shore 7500/9500 Series Hall System User's Manual*,

[Moazed and Nguyen (1988)] 'Ohmic Contacts to Semiconducting Diamond'. K L Moazed , Richard Nguyen . *IEEE Electron Device Letters* July 1988. 9 (7) p. 350.

[Presentation on Highlights from CARAT workshop on Advanced Diamond Detectors] *Presentation on Highlights from CARAT workshop on Advanced Diamond Detectors*,

[Vescan et al. ()] 'Selectively grown ohmic contacts to doped diamond films'. A Vescan , P Gluche , W Ebert , E Kohn . *Electronics Letters* 18th July 1996. 1419. 32 (15) .

[Trew et al. ()] 'The Potential of Diamond and SIC Electronic Devices for Microwave and Millimeter-Wave Power Applications'. Robert J Trew , Jing-Bang Yan & Philip , M Mock . *PROCEEDINGS OF THE IEEE* MAY 1991. 79 (5) .